JOURNAL OF MATERIALS SCIENCE **34** (1999) 2655–2663

Hydrogen storage characteristics of ball-milled magnesium-nickel and magnesium-iron alloys

R. L. HOLTZ, M. A. IMAM
Materials Science and Technology Division, Code 6323, Naval Research Laboratory, Washington, DC 20375, USA
E-mail: holtz@anvil.nrl.navy.mil

Of potential hydrogen storage materials, pure magnesium would be best from the standpoint of hydrogen capacity per unit mass. However, pure magnesium has poor hydriding kinetics. Alloying magnesium with nickel and other transition metals aids catalysis of the hydrogen dissociative chemisorption and yields other benefits by lowering the dehydrogenation temperature, although at the expense of decreased storage capacity. Magnesium-nickel alloys with about one percent nickel prepared by ball-milling yield the most significant improvements in hydrogen storage behavior relative to pure magnesium.

1. Introduction

Magnesium-nickel alloys are used for practical hydrogen storage systems [1, 2]. Pure magnesium has a hydrogen capacity of 7.6 wt % in the form of MgH_2, and this is the highest of any solid hydride except LiH. Pure magnesium, however, is prone to oxidation and low catalytic activity for dissociative chemisorption of H_2, and this limits the hydriding and dehydriding rates. Pure magnesium also has a hydride dissociation temperature (at one atmosphere of hydrogen) of 290 °C, which is marginal for prospective applications. The alloy Mg_2Ni is more stable in air, with a lower hydride dissociation temperature of 250 °C. Nickel significantly improves the catalytic activity, and consequently the hydriding and dehydriding rates are improved, as well. On the other hand, Mg_2Ni has a lower theoretical maximum hydrogen capacity, 3.6 wt %, than magnesium. It is desirable to reduce the nickel concentration in order to increase the hydrogen capacity, but retain the benefits of higher hydriding-dehydriding rates and lower hydriding-dehydriding temperatures.

Magnesium-nickel alloys with compositions as low as 2 at % prepared by mechanical alloying have been reported [3, 4] and have been shown to have high hydrogen capacities and high hydrogen reaction rates compared to both Mg and Mg_2Ni. It has also been shown [5, 6] that small concentrations of dispersed nickel particles prepared by chemical vapor deposition enhance the hydrogen storage characteristics of magnesium. This occurs possibly by altering the surface catalytic activity of the magnesium in contact with nickel particles in a manner similar to that observed for palladium nanoparticles in contact with Mg_2Ni [7].

As suggested above, benefits of small concentrations of nickel in magnesium are realized even if the nickel is present as dispersed particles; i.e., not reacted to form a magnesium-nickel compound. It has been suggested that substituting other transition metals for nickel in Mg_2Ni could increase the hydrogen capacity [8] and perhaps lower the hydride dissociation temperature [9]. Based on these observations, it was decided to explore the behavior of magnesium-iron alloys and compare to results obtained for magnesium-nickel.

2. Synthesis

Alloys of magnesium-nickel and magnesium-iron were prepared using a Union Process ball mill. Commercial Mg ($-20+100$ mesh), and Ni (-100 mesh) or Fe (-100 mesh) powders were milled immersed in mineral oil for 50 hours. Excess oil was poured off, leaving the milled powder damp with oil. The process is described in detail elsewhere [10]. Specimens with nickel concentrations of 0.1, 1, 2.5, 5, and 10 at % and with iron concentrations of 1, 5, and 10 at % were made, along with pure magnesium.

Microstructures of the as-milled materials were examined with a scanning electron microscope (SEM) equipped with an energy dispersive X-ray spectrometer (EDX). The EDX spot size was about 2 μm. Fig. 1 shows backscattered electron micrographs of as-milled Mg-10% Ni and Mg-10% Fe. As seen in the figure, the as-milled materials consist of irregular granules or flakes of gray material generally 5 to 10 μm thick, 10 to 50 μm lateral dimensions. The granules contain embedded particles, the light spots in Fig. 1, generally one tenth to one micron in size. The flakes are larger in the Mg-Fe material than in the Mg-Ni. The EDX was used to study the composition of the granules and particles. Several of the large granules and about a dozen of the small particles were examined in both the Mg-Ni and Mg-Fe specimens. The EDX results are consistent with the granules consisting predominantly of magnesium with the embedded particles predominantly of nickel or iron. Since the SEM/EDX spot size was larger than the particles and their separations, it was not possible to

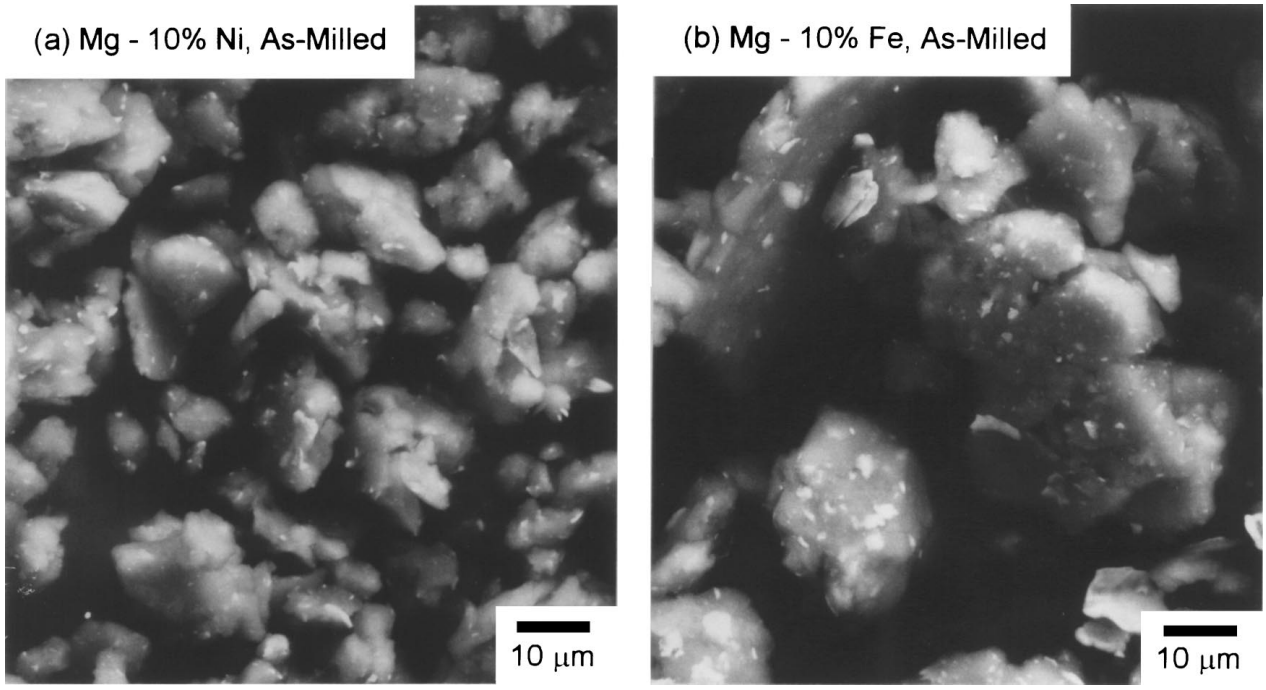

Figure 1 Backscattered electron SEM of as-milled (a) Mg-10% Ni and (b) Mg-10% Fe showing the large granules of Mg with embedded small particles of the Ni or Fe. The grey material making up the bulk of the large granules is predominantly Mg, and the small light spots are particles of (a) nickel or (b) iron.

completely isolate the EDX spectra of the small particles from that of the bulk of the granules. Therefore, the presence of some nickel/iron alloyed with magnesium in the bulk of the granules, or of magnesium in the embedded nickel/iron particles, cannot be ruled out. Some particles of tungsten also were found. These generally were micron-sized, much larger than the nickel/iron particles. The tungsten undoubtedly was the result of residual contamination of the ball mill and stainless steel balls from an earlier project. Tungsten does not absorb significant amounts of hydrogen in the temperature and pressure ranges we studied, so this contamination should not affect the results noticably.

X-ray diffractographs of the as-milled powders, shown in Fig. 2, are unremarkable, showing mostly magnesium and nickel or iron peaks, with some traces of magnesium oxide. All of the Mg-Ni samples show only peaks of Mg, Ni, and MgO in the X-ray diffraction patterns and all Mg-Fe samples show only peaks of Mg, Fe, and MgO. The absence of diffraction peaks of Mg-Ni or Mg-Fe compounds is consistent with the SEM and EDX results described above. It is reasonable to interpret these SEM, EDX, and X-ray diffraction results as indicative of microstructures consisting of magnesium granules with embedded submicron nickel or iron particles.

Portions of the milled product were cold compacted at 900 MPa uniaxial pressure into pellets of one centimeter diameter, with a mass of about one gram each. Densities were measured by hydrostatic immersion. Relative to theoretical densities (assuming a rule of mixtures) the measured densities of both magnesium-iron and magnesium-nickel are similar as a function of transition metal content. For pure magnesium, relative densities of 0.97 were achieved. With increasing transition metal concentration, the relative densities decrease linearly to approximately 0.85 at 10% transition metal content.

3. Hydriding-dehydriding behaviors

Hydriding-dehydriding was carried out on single pellets of the alloys sealed in a thick walled stainless steel tube reaction chamber with a volume of 180 cm^3 and heated with a tube furnace. Thermocouples were attached to the outside of the tube. Digital thermocouple and pressure gauge readouts were interfaced to a computer and the temperature and pressure were monitored and recorded during the hydriding-dehydriding process.

Hydrogen in the reaction system was assumed to behave as an ideal gas. Because the temperature varies throughout the system from room temperature in the external plumbing to close to the furnace temperature in the reaction zone, the equation of state must be integrated over the entire system. A general representation of the gas law for the system with pressure P of N moles of gas, with temperature T and room temperature T_R, is:

$$PV = NRT\Phi(T, T_R), \tag{1}$$

which can be expressed as

$$\Phi(T, T_R) = PT_R/P_RT, \tag{2}$$

where P_R is the pressure at room temperature. The function $\Phi(T, T_R)$ was determined experimentally by measuring pressure and temperature for a chamber without a specimen (so that N is constant) under isothermal conditions for a range of combinations of P, T, and amount of gas (or equivalently, P_0, the pressure at room

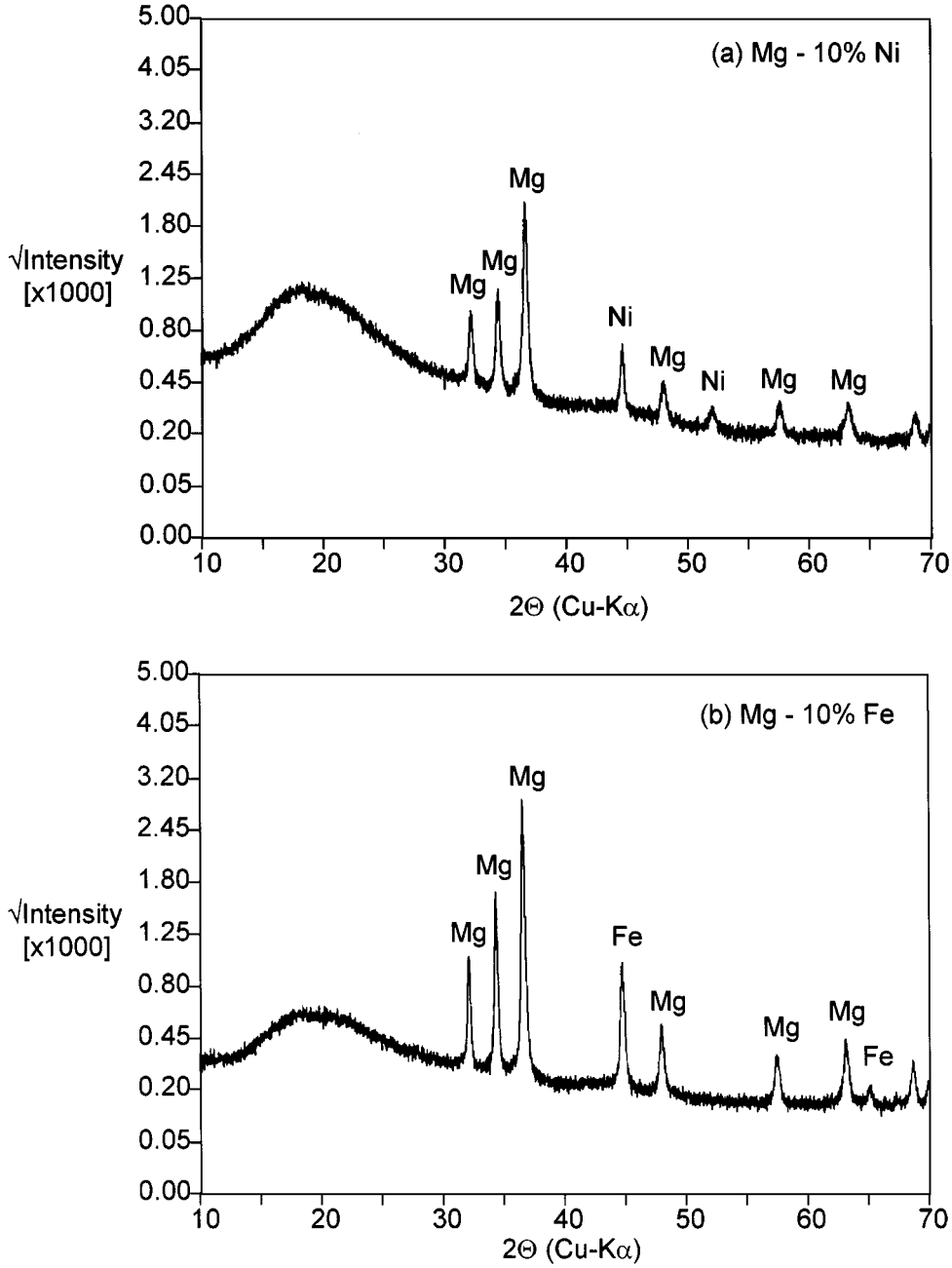

Figure 2 X-ray diffractometer scans of as-milled (a) Mg-10% Ni and (b) Mg-10% Fe.

temperature). For our system, the resulting calibration can be expressed as

$$PV = NR(C_0 + C_1T), \tag{3}$$

where C_0 and C_1 are the experimentally determined calibration constants, 214 and 0.2747, respectively, with both values ±2%.

Fig. 3a and b show the temperatures and pressures as a function of time for a typical rapid thermal cycle with no specimen in the chamber (so that N is constant). The interior gas temperature can be estimated using the measured pressure and the calibration given above, and this estimated temperature versus the measured exterior furnace temperature is plotted in Fig. 3c. There is hysteresis between the measured exterior furnace temperature and the gas temperature inside the chamber. This occurs because of the placement of the thermocouple on the outside surface of the chamber, where it responds more quickly to furnace temperature changes than the interior of the reaction vessel. Using the curve shown in Fig. 3c, the interior gas temperatures during rapid thermal cycling can be estimated from the furnace temperature.

The volume of the reaction system was determined using Boyle's law and a standard volume with an accuracy of 3.5%, and this value was used to scale the effective gas law, Equation 1. At room temperature, a 1.0 MPa pressure change is equivalent to 0.1466 grams of hydrogen absorbed or desorbed. At 350 °C, the conversion factor is 0.1123 grams of hydrogen per MPa. Overall accuracy in hydrogen mass changes is ±5%.

Two types of hydriding-dehydriding procedures were used. Fig. 4a shows the procedure for determining total hydrogen capacity. A dehydrided specimen is heated from room temperature to 350 °C at about 10 °C/min,

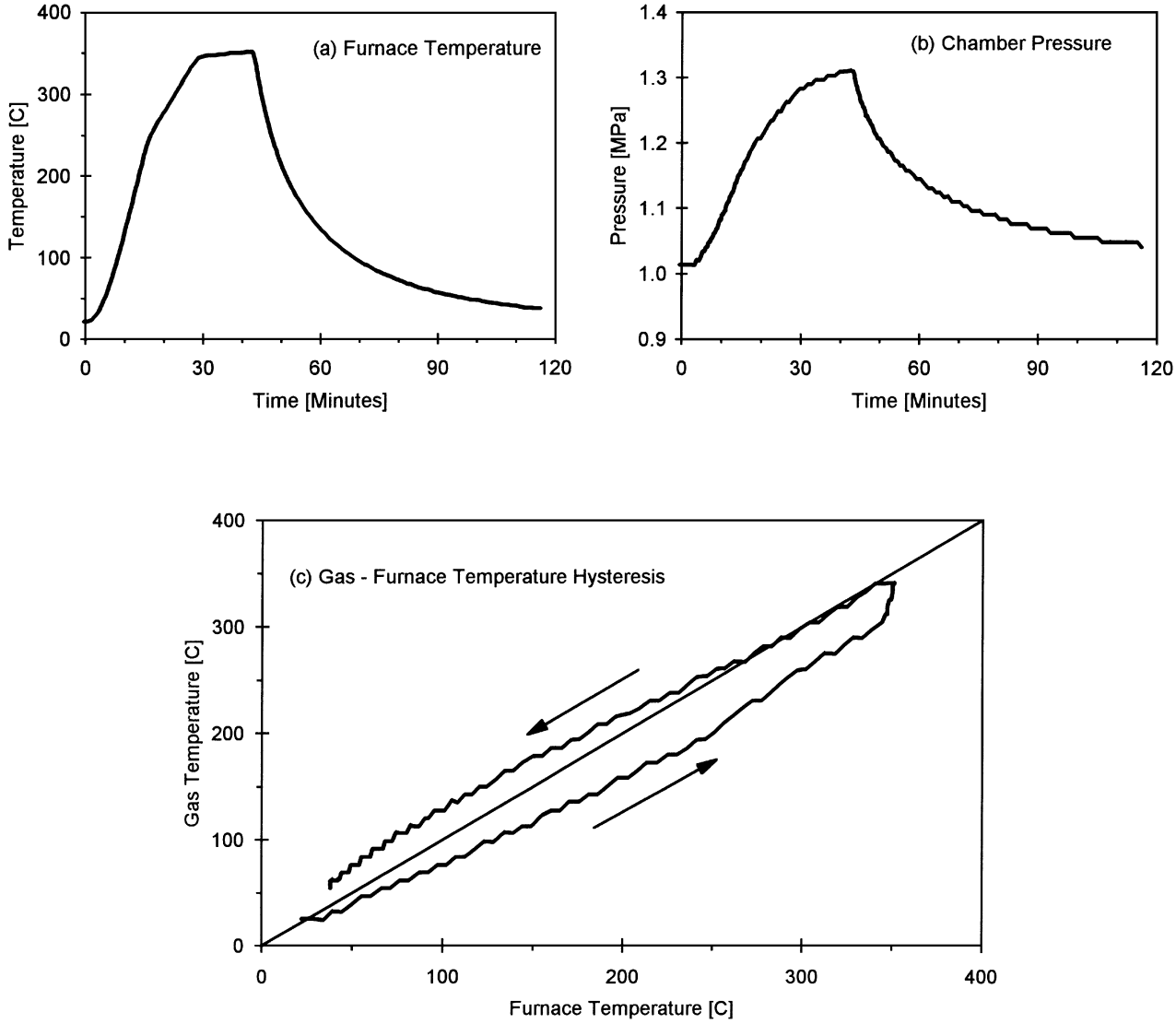

Figure 3 Furnace response during rapid thermal cycling: (a) exterior temperature of the furnace, (b) pressure of the hydrogen gas in the reaction system, and (c) derived relationship of gas temperature inside the reaction zone versus the exterior furnace temperature during rapid thermal cycling.

with an initial hydrogen pressure at room temperature of 1 MPa. The system is then cooled to room temperature. The difference in pressure before and after this heat-cool cycle is due to the total amount of hydrogen absorbed by the specimen. The temperature at which the hydrogen pressure starts to decrease upon the initial heating from room temperature is defined as the "hydrogenation onset" furnace temperature. After cooling to room temperature to determine the pressure change as explained above, the hydrogen gas in the chamber is pumped out and the reactor sealed again. The specimen is not removed from the reactor. The "dehydrogenation onset" furnace temperature is defined as the temperature at which the pressure starts to rise upon heating a fully hydrided specimen starting in vacuum at room temperature.

The second type of cycle, shown in Fig. 4b, was used to evaluate the isothermal dehydriding rates. A specimen is first fully hydrided in 1 MPa of hydrogen at 350 °C. After rapidly reducing the pressure to one atmosphere (0.1 MPa), the increase of pressure as a function of time is monitored as hydrogen evolves from the specimen. The initial slope of the pressure versus time is defined as the "initial hydrogen delivery rate".

The hydrogen capacity of each specimen was measured on the first and sixth cycle, while the other cycles were of the isothermal type described. The hydrogen capacity and onset temperatures were measured on the sixth cycle for all specimens, and the delivery rates were measured on the seventh cycle. This was done because it generally took several cycles for the properties to stabilize completely.

Fig. 5 shows the hydrogen capacity of the Mg-Ni and Mg-Fe alloys in weight percent of hydrogen. Absolute accuracy of the hydrogen capacity shown is about 5% due to the uncertainty in the calibration of the system, but there is negligible uncertainty in the relative capacities of the various specimens.

For the Mg-Ni series, the hydrogen capacity peaks at Mg-1% Ni. The capacity of 6.13 wt % is about 85% of the theoretical maximum capacity for this composition, assuming that a stoichiometric mixture of MgH_2 and Mg_2NiH_4 was obtained. For the Mg-Fe series, the capacity increases linearly with Fe content and the

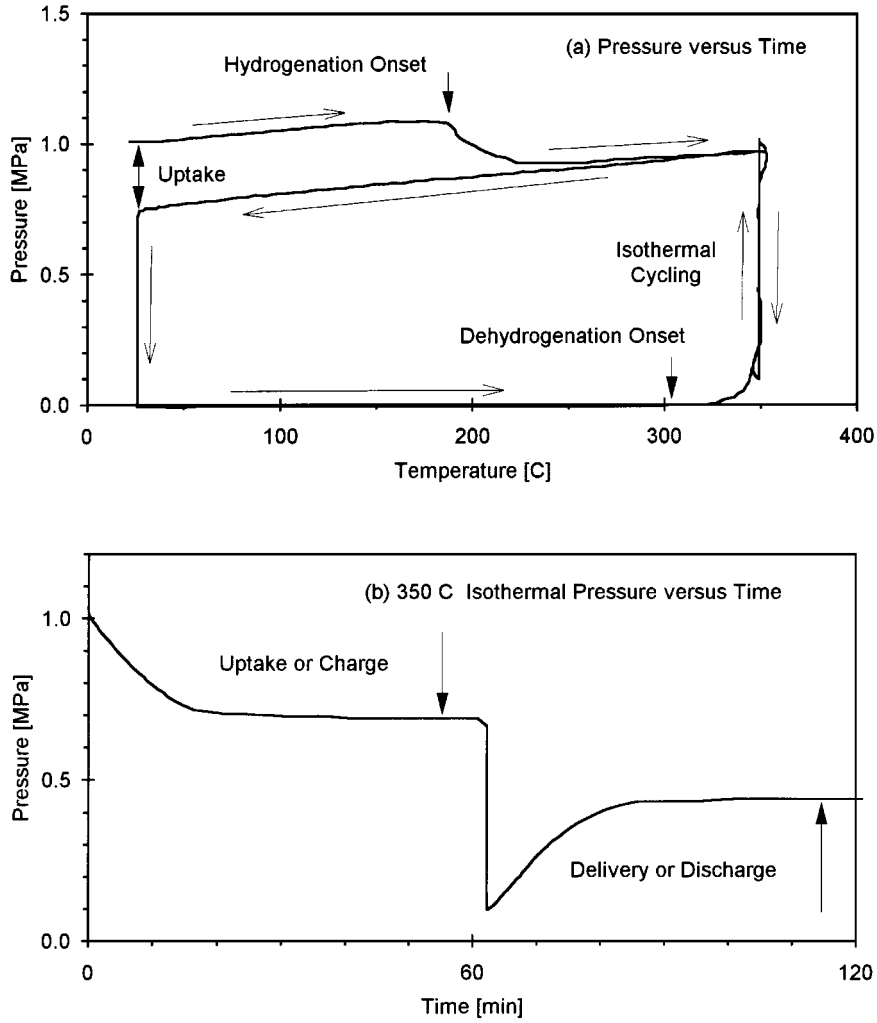

Figure 4 Types of hydride-dehydride cycles used. (a) A rapid thermal cycle starting with 1 MPa of hydrogen at room temperature, increasing the temperature to 350 °C, then cooling back to room temperature, is used to measure total hydrogen capacity. (b) Isothermal cycling at 350 °C is used for measuring hydride-dehydride kinetics.

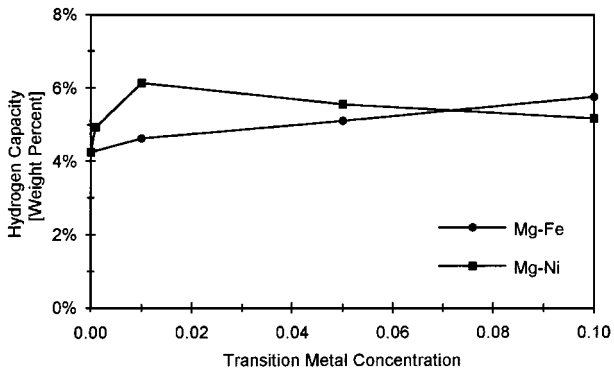

Figure 5 Hydrogen capacity of the ball-milled Mg-Ni and Mg-Fe alloys.

capacity of Mg-10% Fe is slightly higher than that of Mg-10% Ni.

Fig. 6 shows the hydrogen discharge behavior at 350 °C. It shows that as little as 0.1% Ni in Mg improves the discharge rates dramatically, although adding more than 1% Ni yields no additional benefit in the rates. The rates must be limited by a mechanism independent of the nickel content. For 10% Fe in Mg, the discharge curve is comparable to that of 1, 5, or 10% Ni in Mg, again suggesting that the rates are limited by a mechanism independent of the transition metal. However, for 1 and 5% Fe, the discharge is somewhat slower, indicating that Fe is involved in the rate limiting mechanism. This behavior indicates that Ni is more active than Fe in the mechanisms that depend on transition metal, but that above a certain concentration, it does not matter because some other mechanism independent of the transition metal limits the discharge.

Fig. 7 shows the initial hydrogen delivery rates at 350 °C; that is, the rate at which hydrogen can be extracted from the specimen when it is fully hydrided, corresponding to the initial slopes of the curves in Fig. 6. Both Ni and Fe substantially increase the dehydrogenation rates relative to pure Mg, but clearly, Ni is nearly twice as effective as Fe at low concentrations. For Ni concentrations above 1%, the dehydrogenation rate seems to be independent of Ni concentration, while for Fe it increases with concentration. At 10% concentration, both Ni and Fe produce essentially the same effect on dehydrogenation rate.

Related trends are found in the hydrogenation and dehydrogenation onset temperatures versus concentration. While both Ni and Fe result in a lowering of the hydrogenation onset temperature, shown in Fig. 8, there is a large nonlinear effect for Ni. A huge drop of over

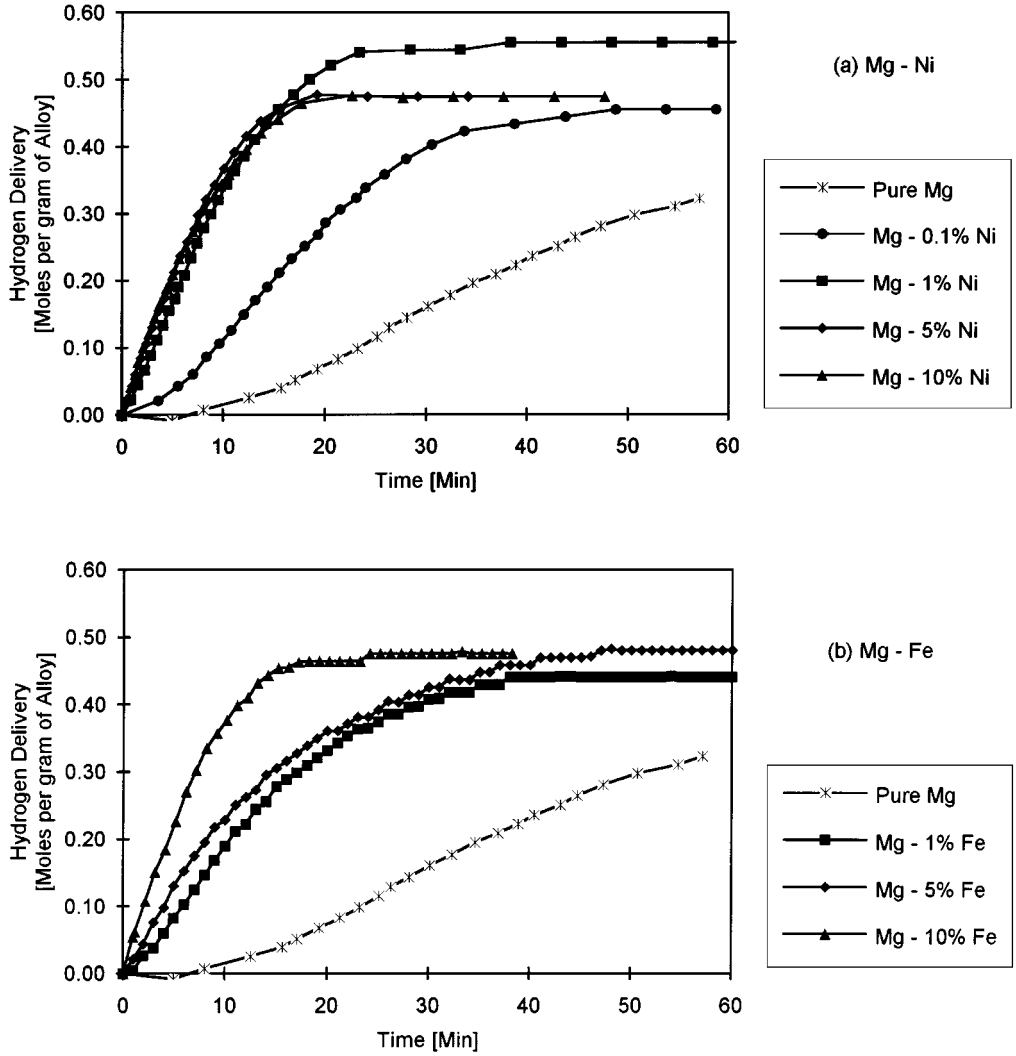

Figure 6 Hydrogen delivery (discharge) versus time at 350 °C after charging with initial 1 MPa pressure. (a) Mg-Ni and (b) Mg-Fe.

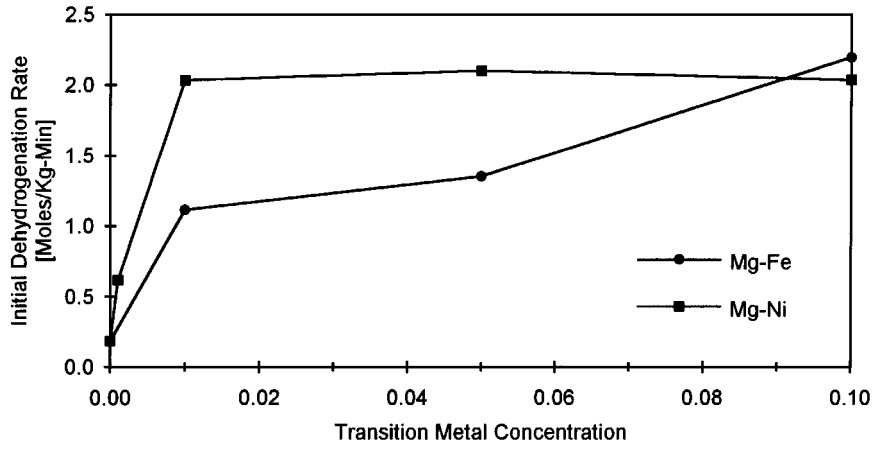

Figure 7 Initial dehydrogenation rates of the Mg-Ni and Mg-Fe alloys at 350 °C.

100 °C in the hydrogenation onset temperature with the addition of just 1% Ni was noted. Further addition of Ni produces further linear change of onset temperature. The same behavior and slope occurs for Fe addition. For the dehydrogenation onset temperatures shown in Fig. 8, there is a large drop of about 50 °C relative to pure Mg for 1% additions of either Ni or Fe. For higher Ni concentration, the dehydrogenation onset temperature seems to be essentially independent of Ni content, but continues to decrease with additional Fe content.

After the hydriding cycles, the pellets, which were initially soft and ductile, were hard, somewhat brittle, and brown in color. Scanning electron micrographs of hydrided Mg-10% Ni and Mg-10% Fe are shown in Fig. 9. Comparing with as-milled powder shown

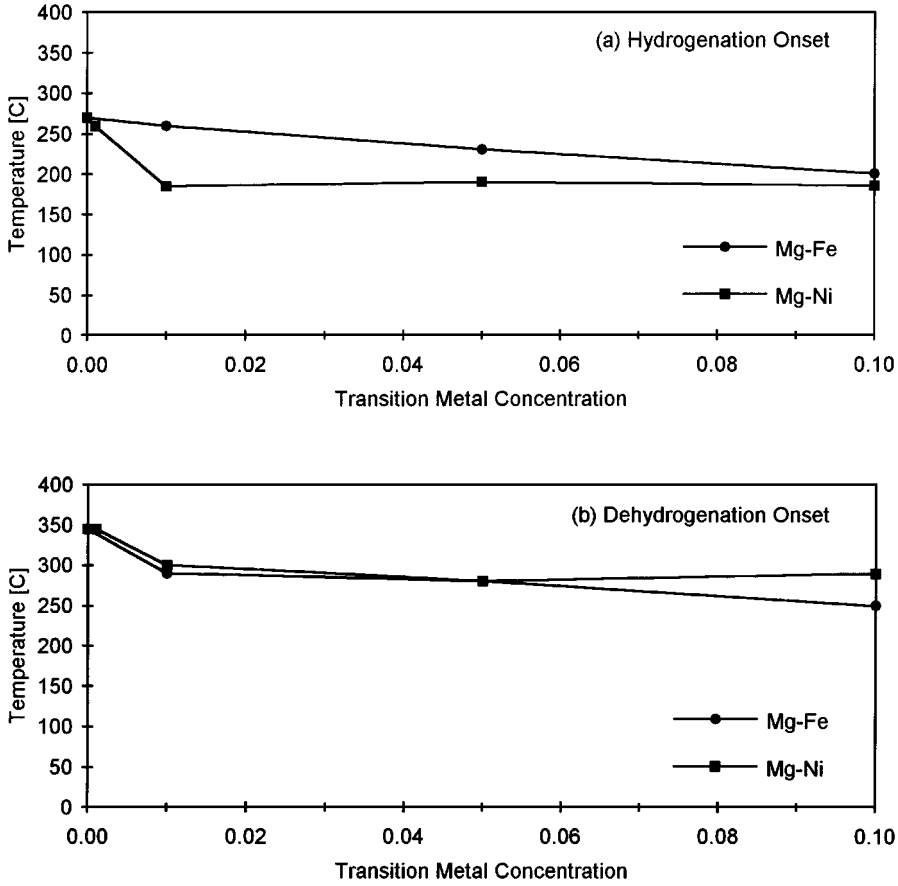

Figure 8 Furnace temperature at onset of (a) hydrogenation and (b) dehydrogenation of Mg-Ni and Mg-Fe alloys in vacuum.

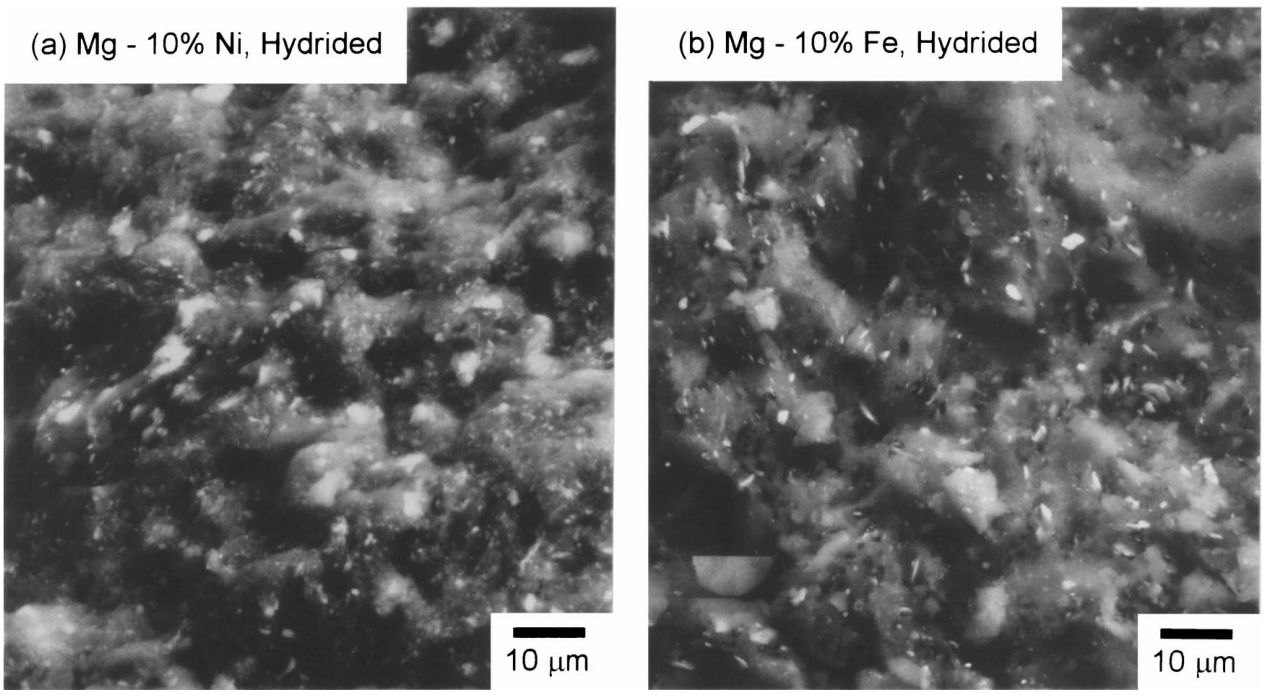

Figure 9 Scanning Electron Micrographs of (a) Mg-10% Ni and (b) Mg-10% Fe after hydriding. Compare with Fig. 1 to see refinement of microstructure.

in Fig. 1, we see that the transition metal or transition metal rich inclusions (the bright particles in these backscattered electron images) are still dispersed throughout Mg. This indicates that Ni or Fe have not fully reacted with the Mg. The scale of the microstructural inhomogeneities are similar in both alloys, and are of the same nature as the as-milled material, except, of course, that the hydrided material has been compacted

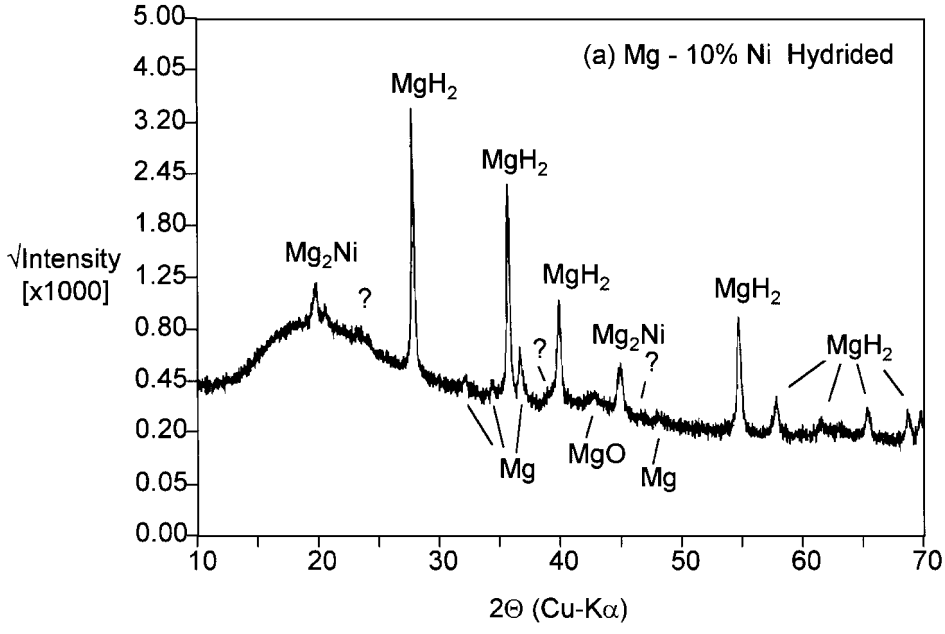

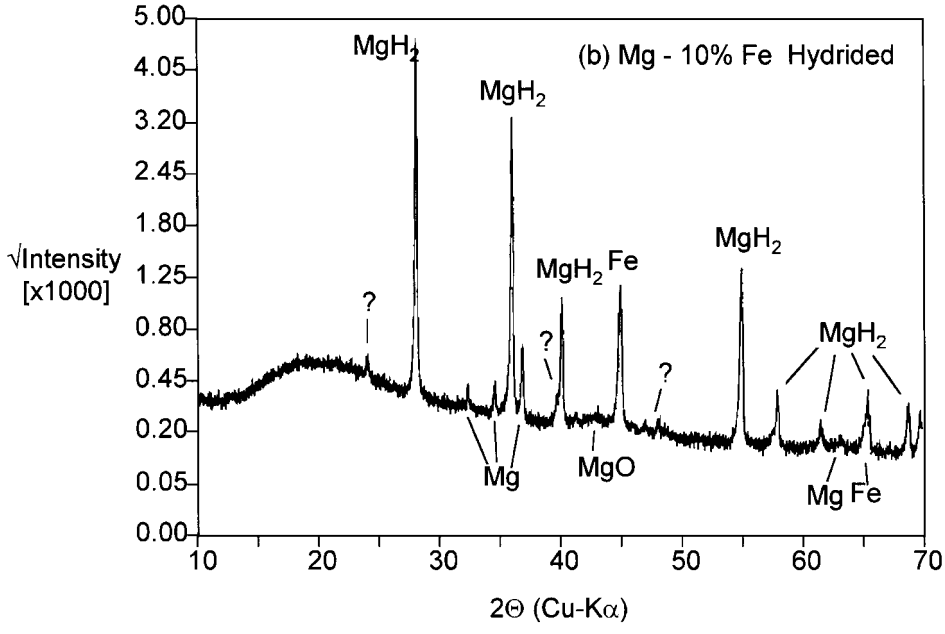

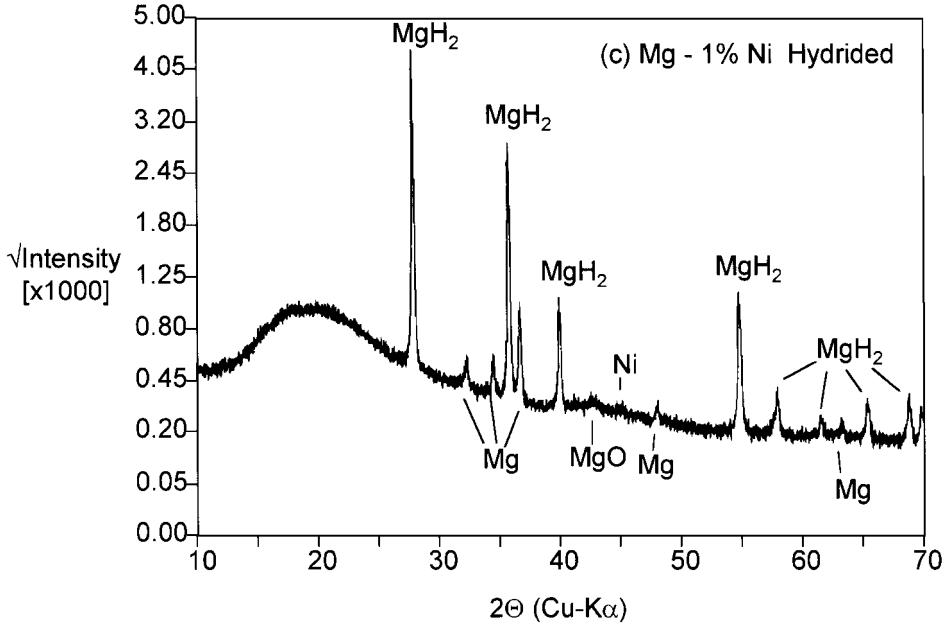

Figure 10 X-ray diffractometer scans of (a) Mg-10% Ni, (b) Mg-10% Fe, (c) Mg-1% Ni, and (d) Mg-1% Fe after hydriding. (*Continued*)

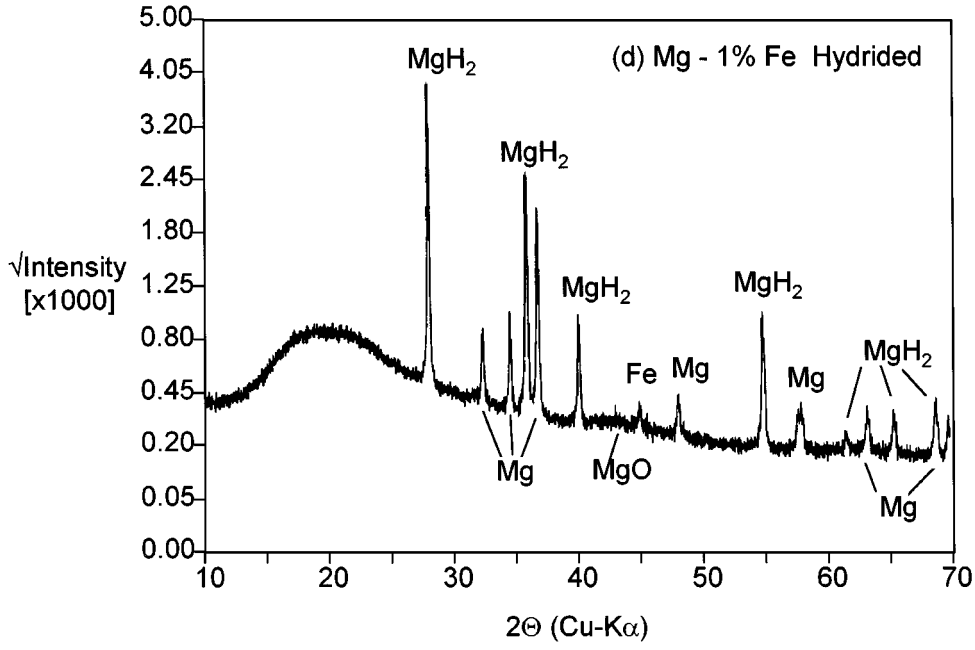

Figure 10 (*Countinued*).

into a pellet. There was no significant degree of pulverization or microstructural refinement, as was found in previous work on alloys with higher transition metal content [10]. Following hydriding, all of the specimens with less than 5% Ni or Fe contain mostly MgH_2 with some Mg, traces of MgO, and Fe or Ni. The Mg-10% Ni specimen also contained some Mg_2NiH_4 and the Mg-10% Fe specimen contained several peaks corresponding to the same phase, presumably Mg_2FeH_4, as shown in Fig. 10

4. Conclusions

Addition of about one atomic percent of nickel to magnesium significantly improves the hydrogen storage characteristics in the following ways: (1) the hydrogen capacity is increased by 50%, (2) the rates of isothermal dehydrogenation are increased by a factor of ten, (3) the temperature for onset of hydrogenation is lowered by nearly 100 °C, and (4) the temperature for onset of dehydrogenation is lowered by nearly 50 °C. No significant additional benefit is attained by increasing the nickel concentration above one atomic percent, and in fact the hydrogen capacity decreases with increasing nickel concentration.

Addition of iron to magnesium have little effect on the hydrogen capacity or the temperature of hydrogenation onset, but increase the dehydrogenation rates by a factor of five relative to pure magnesium. However, iron is only about half as effective as nickel in increasing the dehydrogenation rates. Iron decreases the dehydrogenation onset temperature by about 50 °C, which is about the same effect as obtained with nickel. Unlike nickel, further increasing the iron concentration above one percent results in increased hydrogen capacities, increased dehydrogenation rates and lower dehydrogenation onset temperatures.

The principal role of the transition metal at these low concentrations is to aid dissociative chemisorption of hydrogen. The concentrations are too low to produce significant amounts of magnesium-transition metal compounds. The results described above are consistent with the other rate limiting processes competing with the catalytic activity of the transition metal additions. Nickel is more catalytically active for hydrogen dissociative chemisorption than iron, and even very small concentrations of nickel saturate that part of the process. Some other rate limiting effect, which is independent of nickel concentration, then takes over, probably related to diffusion of hydrogen into the magnesium. Iron, on the other hand, is less active catalytically so that it takes a higher concentration of iron to achieve the same effects as nickel.

Acknowledgement

The authors thank Mr. Keith Robinson for performing the ball-mill synthesis.

References

1. J. J. REILLY and G. D. SANDROCK, *Scientific American* **242** (1980) 98.
2. D. L. DOUGLASS, *Metall. Trans. A* **6A** (1975) 2179.
3. M. Y. SONG, *Int. J. Hydrogen Energy* **20** (1995) 221.
4. M. Y. SONG, *J. Mater. Sci.* **30** (1995) 1343.
5. H. IMAMURA, Y. MURATA and S. TSUCHIYA, *J. Less-Common Metals* **135** (1987) 277.
6. H. IMAMURA, Y. USUI and M. TAKASHIMA, *ibid.* **175** (1987) 171.
7. L. ZALUSKA, A. ZALUSKA, P. TESSIER, J. O. STROM-OLSEN and R. SHULZ, *Journal of Alloys and Compounds* **217** (1995) 295.
8. P. SELVAM, B. VISWANATHAN, C. S. SWAMY and V. SRINIVASAN, *Int. J. Hydrogen Energy* **13** (1988) 87.
9. J. P. DARNAUDERY, B. DARRIET and M. PEZAT, *ibid.* **8** (1983) 705.
10. R. L. HOLTZ and M. A. IMAM, *J. Mater. Sci.* **32** (1997) 2267.

Received 6 October 1997
and accepted 15 December 1998